

Ion-crystal demonstration of a temperature-driven structural phase transitionJ. Li,^{1,2} L. L. Yan,^{1,3,*} L. Chen,^{1,†} Z. C. Liu,^{1,2} F. Zhou,¹ J. Q. Zhang,¹ W. L. Yang,¹ and M. Feng^{1,4,‡}¹*State Key Laboratory of Magnetic Resonance and Atomic and Molecular Physics, Wuhan Institute of Physics and Mathematics, Chinese Academy of Sciences, Wuhan 430071, China*²*School of Physics, University of the Chinese Academy of Sciences, Beijing 100049, China*³*School of Physics and Engineering, Zhengzhou University, Zhengzhou 450001, China*⁴*Department of Physics, Zhejiang Normal University, Jinhua 321004, China*

(Received 10 September 2018; published 5 June 2019)

Thermal fluctuation usually damages observations in physical systems. But here we demonstrate a unique contribution made by thermal fluctuation, that is, our observation of linear-zigzag phase transitions induced solely by temperature of the $^{40}\text{Ca}^+$ ion crystals in a surface-electrode trap. In contrast to the previously observed counterparts based on change in the mechanical equilibrium conditions of the ions, our presented structural phase transition occurs due to controllable influence of thermal fluctuation. The ions' temperature is well controlled by tuning the cooling laser and the experimental observation could be fully understood by classical Langevin equation in addition to the effects from thermal fluctuation. Our experimental investigation indicates the possibility of the positive role thermal fluctuation played in the thermodynamic process at the atomic level, which might bridge the thermodynamics from the macroscopic domain to the quantum regime.

DOI: [10.1103/PhysRevA.99.063402](https://doi.org/10.1103/PhysRevA.99.063402)**I. INTRODUCTION**

With advances of laser cooling techniques, observing the thermodynamic process in few microscopic particles, e.g., trapped ions, in cryogenic situation is currently available [1–4]. In contrast to the conventional thermodynamics applied in macroscopic systems, microscopic thermodynamics has displayed considerable differences, ranging from violation of the basic thermodynamic laws to the redefinition of thermodynamic quantities [5].

Dynamics of microscopic particles is strongly influenced by thermal fluctuation, which is generally regarded as a detrimental effect. But in the present work, we demonstrate an experiment relevant to configurational variation of cold ion crystals confined in an electromagnetic potential, in which thermal fluctuation could act positively. Our observation belongs to cryogenic phase transition regarding self-organized matter [6–8]. The critical behavior in such phase transitions occurred usually due to variation of characteristic parameters of the systems, which could be fully explained by classical physics [9]. These observations, including complex changes of the crystalline configuration [10–15], reflect the roles of nonlinearity and long-range order played in many-body physics. Understanding these characteristics is one of the indispensable prerequisites to the control of dynamics of the complex system at the microscopic level.

What we have observed is a temperature-driven structural phase transition (SPT) in an ion-crystal system, which is a

transformation between the linear structure and the zigzag, belonging to the configurational variation mentioned above [10–15]. Such configurational variations were conventionally observed by changing mechanical equilibrium conditions of the ions. However, the crystalline configuration in our case varies due to controllable change of thermal fluctuation experienced by the ions. Since this fluctuation effect is very feeble and hard to precisely control, generating such a SPT has never been explored before. In fact, this fluctuation effect had also been neglected in previously theoretical studies focusing only on mechanical effects in the laser-ion interaction and Coulomb repulsion, and thus the experimental investigations in this aspect were based on the change of mechanical conditions, such as the trapping potential, e.g., our previous observation [16]. Actually, the thermal fluctuation (even quantum fluctuation) effect, although very weak, is another possible factor which could vary the structures of the ion crystals, as predicted in [17]. Since this fluctuation effect can be reflected by the ions' temperature, the associated SPT is called temperature-driven SPT, which occurs at the ions' temperature ranging from 1 mK to tens of mK [17].

Our observation focuses on the linear-zigzag variation of seven laser-cooled $^{40}\text{Ca}^+$ ions, due to controllable change of temperature, in a surface-electrode trap, as sketched in Fig. 1. The trap is a 500- μm scale planar trap with five electrodes made of copper on a vacuum-compatible printed circuit board substrate. The details of the trap potential could be found in [16]. One particular point worth mentioning here is the strong asymmetry in the trap, where the potential well in the y axis is much steeper than in both x and z axes, leading to the ion crystals distributed only in the xz plane. So the anisotropic parameter $\alpha = \omega_x/\omega_z$, with $\omega_x(\omega_z)$ being the trap frequency in the $x(z)$ axis, is an important quantity, whose

*qingnuanbinghe@126.com

†liangchen@wipm.ac.cn

‡mangfeng@wipm.ac.cn

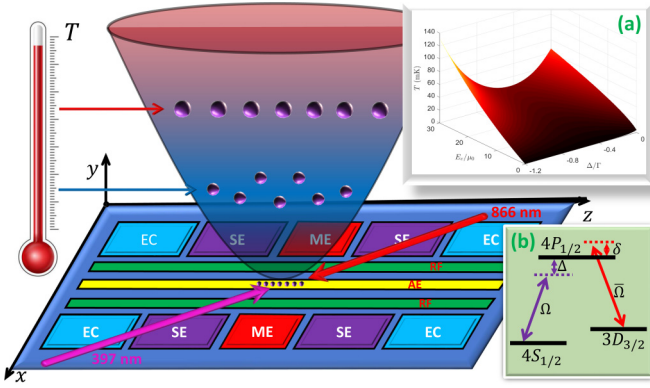


FIG. 1. Schematic of the surface-electrode trap and the SPT. The trap is composed of a central electrode (AE), two rf electrodes (RF), and two outer segmented dc electrodes. Each of the outer segmented dc electrodes consists of five component electrodes, i.e., a middle electrode (ME), two control electrodes (SE), and two end electrodes (EC). The paraboloid above the trap plane presents a magnified diagram of a harmonic potential for seven crystalline ions varying structure with respect to the temperature T . (Inset) (a) Temperature T of the ion crystals relying on both the detuning Δ of the cooling laser and the bath heating intensity E_e in units of $\mu_0 = 1 \times 10^{-21} \text{ N}^2\text{s/kg}$, and (b) 397-nm laser drives the transition between the excited state $|4P_{1/2}\rangle$ (lifetime 7.1 ns) and the ground state $|4S_{1/2}\rangle$, which plays the main role of cooling, and 866-nm laser couples $|4P_{1/2}\rangle$ to the metastable state $|3D_{3/2}\rangle$ for repumping the 6% leakage of spontaneous emission back to $|4P_{1/2}\rangle$. The detunings Δ and δ are defined as the frequency differences of the lasers from the two-level resonance.

variation over the transition point α_c drives the system to cross from one phase to the other [16]. In our case here, under the condition of $\alpha > 3.14$, the ion crystals behave as one (line) or two (zigzag)-dimensional configurations in the xz plane with the thickness less than $2 \mu\text{m}$ along the y axis. Our observation along the y axis could obtain full information about the crystalline structural changes.

II. ANALYTICAL EXPRESSION OF THE ION CRYSTALS' TEMPERATURE

For our purpose, the key point of our implementation is the capability to controllably adjust the ions' temperature, which is relevant to the friction due to the cooling laser in this work. As defined in Appendix A, the friction coefficient produced by the cooling laser is given by

$$\beta = 4\Omega^2\Gamma_1 k_1 \cos^2\theta \left(\frac{N_2}{N} - \frac{N_1}{N^2} \right), \quad (1)$$

where Ω and Γ_1 are, respectively, the Rabi frequency and the linewidth regarding the excited state $|4P_{1/2}\rangle$, and k_1 is the wave number of the 397-nm cooling laser which irradiates the ions with respect to the z axis by θ . N , N_1 , and N_2 in Eq. (1), as defined in Appendix A, are functions of the detunings Δ and δ . Moreover, it is usually impossible to estimate the Rabi frequency in the Doppler cooling due to the short lifetime of the excited state $|4P_{1/2}\rangle$. To overcome this difficulty, we have proposed a practical method based on the relationship

of the Rabi frequency with the detuning, as presented in Appendix B.

In our trap system, the bath heating comes from rf heating, Johnson noise in addition to some anomalous heating [18], where Johnson noise is the thermal electron noise in the resistance of the electrodes and the anomalous heating is still of unclear mechanism [19]. For convenience of the treatment below, we leave all these noise to the bath heating strength E_e , and thus the ions' temperature T after the Doppler cooling can be written as

$$T = \frac{(\Delta - \delta)^2}{k_B N_h} + \frac{mE_e}{2k_B\beta}, \quad (2)$$

where the first term represents the heating effect due to photon scattering with the detuning-dependent N_h defined in Appendix A and the second term is regarding the bath heating. Here we have assumed uniform temperature of each of the ions in different vibrational directions based on the results in [20]. With the above equations, we find that the temperature can be fully controlled by the detuning Δ for a certain bath heating strength, as plotted in Fig. 1(a).

III. EXPERIMENTAL OBSERVATION OF THE TEMPERATURE-DRIVEN SPT

Our experimental setup is located in a vacuum chamber at room temperature. The ions' temperature is relevant to their vibration controlled by lasers. As such, to ensure a high-quality demonstration of this temperature-driven SPT, we have locked, before experimental implementation, both the 397-nm and 866-nm lasers to an optical cavity made of a material with ultralow expansion, and also employed the Pound-Drever-Hall technique. The incident directions of both the lasers are nearly parallel to the trap surface to minimize the scattering light due to the laser beams striking the surface of the trap, where the 866-nm laser with a small angle of $\pi/36$ with respect to the xz plane provides a small component of the cooling effect in the y axis [21]. The powers of 397-nm and 866-nm lasers are, respectively, $40 \mu\text{W}$ and $250 \mu\text{W}$, which yield $\Omega/\tilde{\Omega} = 0.4$. Besides, we have tried, by adjusting the compensation voltage V_{AE} , to keep the ion crystals initially close to the rf potential null, following the idea in [22]. We find by minimizing ions' excess micromotion by modulating rf voltage that the ions are least influenced by the rf heating when they are located along the z axis and above the trap surface by $910 \mu\text{m}$. Moreover, our experiment gets started from the critical region of the SPT, which is obtained by checking a wide range of the parameters in advance by sweeping α , as clarified later.

In the experiment, we confine seven ions in the surface-electrode trap by Doppler cooling, and then exactly raise the trapping potential to $\alpha = 3.205$, which is accomplished by adiabatically increasing the voltage on the ME electrodes. We sweep the detuning Δ of the 397-nm laser from -120 MHz to 0 MHz , during which the ion crystals experience a weak-strong-weak variation of the cooling efficiency, inducing a structural change from the linear to the zigzag and then back to the linear, as shown in Fig. 2. The resolution blurring of the ions' images in our observation is mainly due to thermal effect of the ions resulting from the finite temperature (10–65 mK).

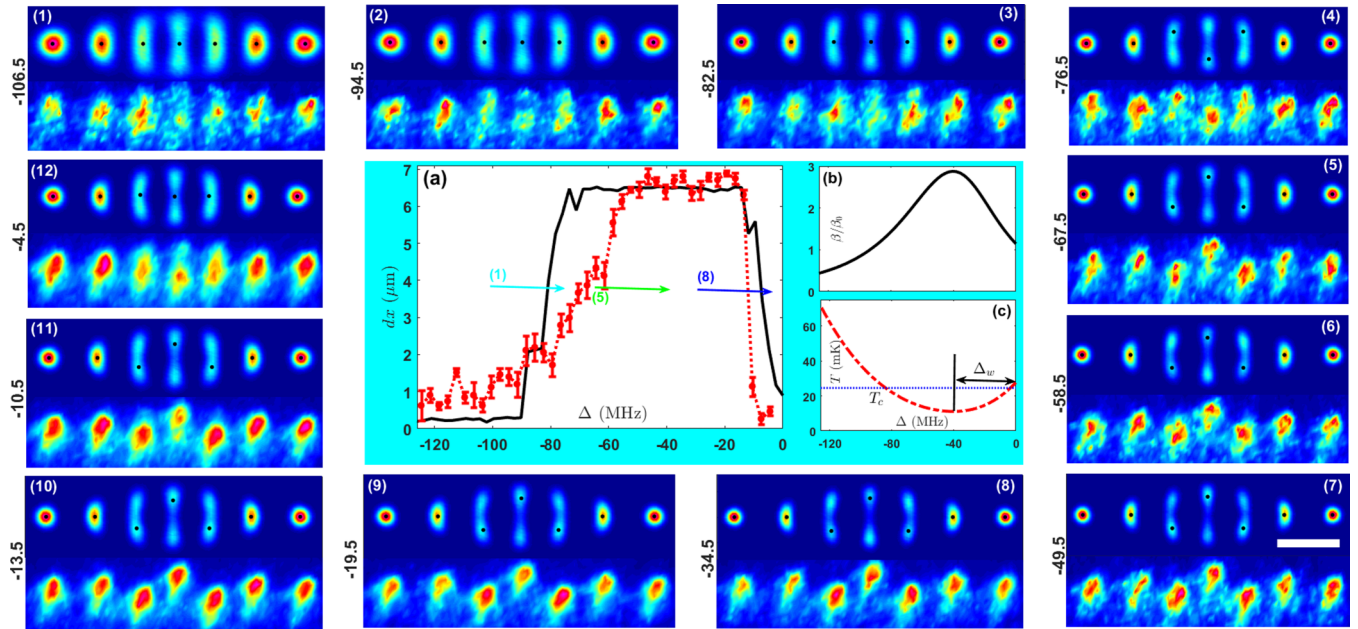


FIG. 2. SPT of seven $^{40}\text{Ca}^+$ ion crystals induced by the detuning Δ of the cooling laser. (a) Order parameter dx in variation with the detuning, where the experimental observation (red dotted curve) is fitted by the numerical simulation (black solid curve) and the error bars of the experimental data (measured by 50 repetitions) are determined by the mean square root. (b) Friction coefficient β in units of $\beta_0 = 1 \times 10^{-21}$ Ns/m as a function of the detuning Δ . (c) Temperature T of the ion crystals in the xz plane varying with the detuning Δ , where Δ_w denotes the width of the detuning window, defined as the detuning difference from the point of zero friction coefficient to the point of the largest, and the blue dashed line indicates the critical temperature T_c . The panels (1)–(12) present experimentally observed images (the lower of each panel) in comparison with numerically simulated results (the upper of each panel), where the number in the vertical axis of each panel is the detuning Δ in units of MHz, corresponding to the phase transition steps labeled in (a). The horizontal direction means the z axis, the anisotropic parameter $\alpha = 3.205$, and the bath heating intensity $E_e = 13\mu_0$. A $20\text{-}\mu\text{m}$ scale bar is drawn in panel (7) by considering the CCD resolution and 15 times magnification of the microscope objective before the CCD imaging. The scale bar applies to all the images.

Nevertheless, considering the center of each ion, we could still identify the configurations of the ion crystals by means of a practical method (see Appendix C).

Figure 2 indicates the observed configuration changes of the ion crystals in good agreement with the simulated results by the Langevin equation (see Appendix D). To characterize the structural changes, we employ the center-to-center distance dx of the two outermost ions in the x axis as the order parameter, which is very sensitive to the temperature change. As shown in Fig. 2(a), we find an abrupt raising in the curves of dx with respect to Δ around $\Delta_c = -84$ MHz and an abrupt falling around $\Delta_c = -5$ MHz, implying, respectively, the SPTs from the linear to the zigzag and back to the linear. Based on the analytical results in Appendix D, we may fully understand the phase transitions induced by the variations of the friction coefficient and the ions' temperature; see Figs. 2(b) and 2(c). The critical temperature is $T_c = 24(2)$ mK for both the abrupt rising and falling. The strongest friction of the cooling laser and the lowest temperature of the ion crystals appear at $\Delta = -40$ MHz, implying that the zigzag structure occurs at lower temperature than the linear chain. This is also reflected in the observation that the ions in the zigzag phase present clearer pictures even though those ions deviated from the z axis should suffer more serious rf heating. Considering all these associated factors, we deem that the laser cooling is dominant in this phase transition process.

IV. SCALING BEHAVIOR OF THE TEMPERATURE-DRIVEN SPT

To give a more complete impression on this topic, we should fully characterize the scaling behavior at different transition points, which is also the prerequisite of understanding the present experiment. To this end, we have explored a wide range of Δ and α for the critical behavior of the phase transition (Fig. 3). Although the strong bath heating makes the observation of the critical region blurry and deviated somewhat from numerical simulation, the experimentally obtained phase diagram could be in principle explained by numerical results from the molecular dynamics method based on the Langevin equation. For example, we present particularly the comparison between experimental observation and theoretical simulation for the critical region of the abrupt rising [see the red dots in Figs. 3(a) and 3(b)], which means that the anisotropic parameter α determines the critical detunings. In fact, α also determines the corresponding critical temperature, as plotted in Fig. 3(c). As predicted in [17], the SPT occurs due to condensation of phonons into the soft mode—the lowest frequency collective motional mode of the ion crystals, which produces a linear scaling law between the critical temperature T_c and the anisotropic parameter α . Our observation in Fig. 3(c) shows that the soft mode exists in the zigzag configuration, conforming to the previous prediction

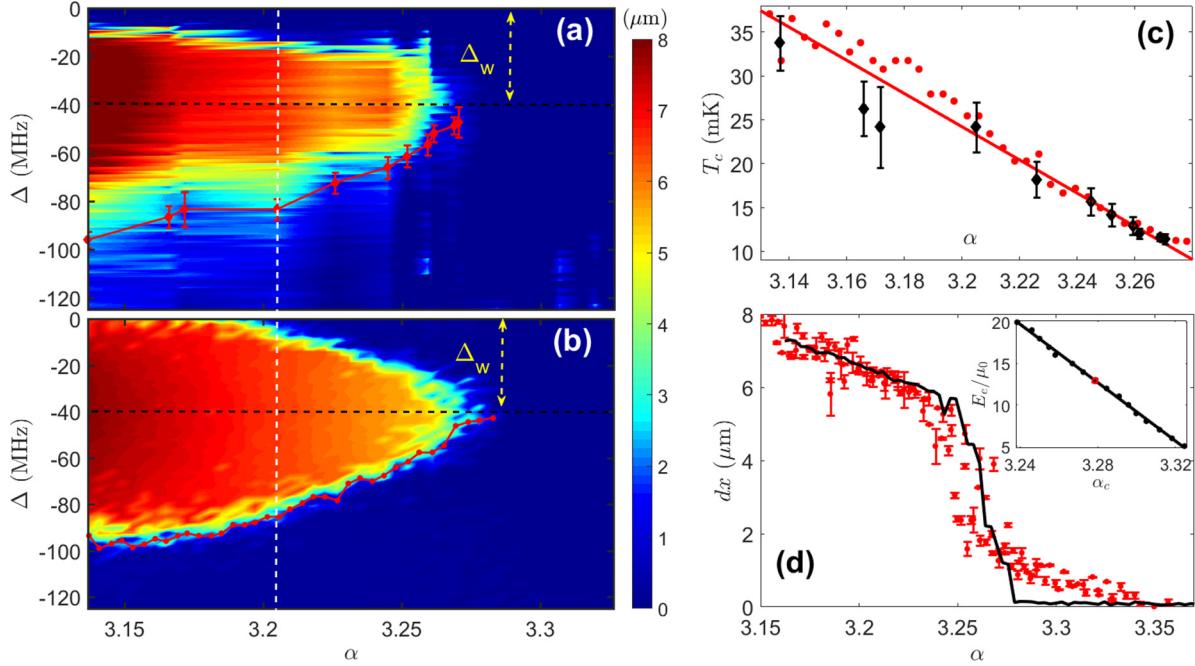


FIG. 3. Experimental observation of SPT. (a) and (b) Phase diagrams of the SPT with respect to the detuning Δ and the anisotropic parameter α , where the color bar indicates the values of dx . The vertical white dashed line labels the location of the observation demonstrated in Fig. 2. The horizontal black dashed line indicates the position of the maximum order parameter dx . Δ_w denotes the width of the detuning window, as labeled in Fig. 2(c). The red-dot curves in (a) and (b) denote the critical detuning of SPT for different α . (a) Experimental observation with each data measured by 50 repetitions. (b) Numerical simulation with the bath heating intensity $E_e = 13\mu_0$. (c) Critical temperature T_c of the SPT vs α , where red dots and black diamonds are obtained, respectively, by numerical simulation in (b) and experimental measurements in (a), and the red line is a linear fitting of the numerical results with $T_c = -189\alpha + 629$. (d) Experimental observation of the SPT by sweeping α for $\Delta = -30$ MHz, where dots are experimental data measured by 20 repetitions, and the black solid curve is a numerical simulation with the transition point estimated as $\alpha_c = 3.279(4)$. The error bars indicate standard deviation. (Inset) Bath heating intensity E_e as a function of α_c in the case of $\Delta = -30$ MHz, where dots are obtained by numerical simulation and the line denotes a linear fitting with $E_e/\mu_0 = -176.3\alpha_c + 591$. The red circle indicates the transition point in our experiment.

[17,23]. As happened in finite temperature, the critical behavior is strongly sensitive to the thermal effects, which lead to anharmonic coupling between different phonon modes. The higher temperature of the ions brings about more complicated phonon coupling, implying more challenge to identify the phase transition critical behavior. Thus, in Fig. 3(c), there are larger errors and deviation observed at the higher temperature.

Besides, we should also measure the bath heating strength before implementing the phase transition. The theoretical study, as presented in Appendix E, has shown a linear relation of the phase transition point α_c with E_e , implying that E_e can be measured by experimentally observing the position of critical point α_c [Fig. 3(d) inset]. In Fig. 3(d), we choose $\Delta = -30$ MHz and find the transition point $\alpha_c = 3.279(4)$, which gives $E_e = 13.0(8)\mu_0$. As such, temperature T in our experiment can be indirectly detected based on Eq. (2), for which Ω is obtained by measuring Δ_w in a linear relation presented in Appendix B. With this method, we obtain $\Omega = 78(17)$ MHz by measuring $\Delta_w = 40(6)$ MHz in Fig. 3, and thus T is obtained.

V. DISCUSSION

Estimating temperature of the ions is essential to our investigation of the temperature-driven SPT. Unfortunately, there has been no working way to accurately detect tem-

perature of the trapped ions in the Doppler cooling. Our proposal to estimate the ions' temperature is based on the ions' spontaneous emission, the bath heating, and the friction due to laser cooling, as explained in Appendix A. This is a standard treatment from the viewpoint of energy to assess temperature of cold atoms. A key point worth mentioning is the bath heating intensity E_e , which is assumed to be a constant in our simulation due to the following facts. First, during the experiment, no change has ever been made on the dc voltage as well as the rf power and frequency regarding the trap. Second, after finishing each SPT, we monitored the temperature of the ions by sweeping the frequency of the cooling laser (i.e., 397-nm laser) on the ions. Under the same mechanical equilibrium condition, we observed unchanged temperature of the ions for SPT occurrence each time. Third, as mentioned above, the laser cooling is dominant in the SPT process. So we may reasonably assume that the bath heating variation for different ion structures is negligible in our Doppler cooling process.

The discrepancy between the experimental values and the simulated results indicates the imperfection in our operations with respect to the ideal consideration. Compared to the rf heating and anomalous heating, the heating due to the thermal bath of the ions is the main source of errors, which keeps bringing in thermal noise and leads to measurement imprecision. Besides, it was reported [19] that the noise in-

duced by black-body radiation could be much enhanced in the presence of a surface than in the free space. According to our estimate, however, such noise above our trap surface at room temperature is smaller than other sources of noise observed by 10^5 times, implying negligible influence. In the above figures, part of the influence due to bath heating on the measurement is left to the error bars as statistical errors, and others yield the experimental values deviated from the simulated results.

For the Doppler cooling applied on a multilevel system, dark resonance [24–26] usually occurs in the fluorescence spectrum and thereby the cooling efficiency is related to many factors [27,28]. Dark resonance is observed in the Doppler cooling of the $^{40}\text{Ca}^+$ ion when the detunings of the 397-nm laser and the 866-nm laser are equal, which lowers the cooling efficiency [29]. To avoid the complexity due to dark resonance in our case, we set the 397-nm laser only at the red-detuning side, but keep the 866-nm laser slightly blue-detuned throughout the experiment, the latter of which is practically accomplished by sweeping the 866-nm laser to the point that the cooling starts weakening. This makes sure that the cooling efficiency is strongly relevant to the detuning of the 397-nm laser, and thus the temperature of the ions is strictly controlled by tuning the frequency of the 397-nm laser.

VI. CONCLUSION

Our observation of linear-zigzag pattern change in ion crystals under controllable influence of thermal fluctuation is a witness of positive contribution from the thermal effect in a microscopic thermodynamic process. Different from the temperature-relevant cloud-order phase transitions in ion traps as observed previously in [30–32], the trapped ions in our case have just changed the crystalline conformation throughout the experimental process. More importantly, our observation of bidirectional changes between the linear and zigzag structures undoubtedly indicates that thermal fluctuation could play an essential role, even a positive role, in microscopic thermodynamics, which could never have been understood in the conventional thermodynamics regarding the macroscopic systems. As such, the trapped-ion system in conformation variation provides a good research platform for reconsidering thermodynamic quantities and processes subject to the fluctuation theory [33,34]. Further cooling of the ion crystals down to zero temperature would yield the SPT under consideration mapping into a quantum phase transition of the transverse-field Ising model [35–37]. Then more observations under quantum fluctuation from the classical to quantum phase transition could be expected [38,39].

ACKNOWLEDGMENTS

This work was supported by National Key R&D Program of China under Grant No. 2017YFA0304503, by National Natural Science Foundation of China under Grants No. 11835011, No. 11804375, No. 11734018, No. 11674360, and No. 91421111, and by the Strategic Priority Research Program of the Chinese Academy of Sciences under Grant No. XDB21010100.

APPENDIX A: FRICTION COEFFICIENT IN DOPPLER COOLING

The trapped $^{40}\text{Ca}^+$ ion in the Doppler cooling works as a three-level configuration coupled by two lasers, as sketched in Fig. 1, where the 397-nm laser drives the transition between the excited state $|4P_{1/2}\rangle$ and the ground state $|4S_{1/2}\rangle$, which plays the main role of the cooling, and the 866-nm laser couples $|4P_{1/2}\rangle$ to the metastable state $|3D_{3/2}\rangle$ for repumping the 6% leakage of spontaneous emission back to $|4P_{1/2}\rangle$ which means the ratio $\Gamma_2/\Gamma_1 = 0.064 \ll 1$. For simplicity, our analytical treatment below focuses on the limit of $\Gamma_2/\Gamma_1 \rightarrow 0$. In the interaction picture, the Hamiltonian for z -axis motion is given by ($\hbar = 1$),

$$H' = \Delta|1\rangle\langle 1| + \delta|2\rangle\langle 2| + \frac{\Omega}{2}(|3\rangle\langle 1|e^{ik_1z\cos\theta} + \text{H.c.}) + \frac{\bar{\Omega}}{2}(|3\rangle\langle 2|e^{-ik_2z\cos\theta\cos\bar{\theta}} + \text{H.c.}), \quad (\text{A1})$$

where the detunings $\Delta = \omega_1 + \omega - \omega_3$ and $\delta = \omega_2 + \bar{\omega} - \omega_3$, the operator $\sigma_x^{ij} = |i\rangle\langle j| + |j\rangle\langle i|$ ($i, j = 1, 2, 3$), ω_i represents the energy of the state $|i\rangle$, ω ($\bar{\omega}$), and Ω ($\bar{\Omega}$) are the corresponding frequency and Rabi frequency of the 397-nm (866-nm) laser with wave number k_1 (k_2). As shown in Fig. 1, the 397-nm laser beam is in parallel with the xz plane with the angle of $\theta = \pi/4$ with respect to the z axis and the 866-nm laser shines in an opposite direction with the angle of $\bar{\theta} = \pi/36 \ll 1$ with respect to the xz plane. Using the relation $\langle F \rangle = -\langle \nabla H' \rangle$, in the limit $k_1z\cos\theta \ll 1$ and $k_2z\cos\theta\cos\bar{\theta} \ll 1$, we obtain the average force as

$$\langle F \rangle = -\frac{\Omega k_1 \cos\theta}{2} \text{Tr}[\rho_s \sigma_y^{13}] + \frac{\bar{\Omega} k_2 \cos\theta \cos\bar{\theta}}{2} \text{Tr}[\rho_s \sigma_y^{23}], \quad (\text{A2})$$

where ρ_s is the steady state of the three-level system. Straightforward deduction yields, in the limit $\Gamma_2/\Gamma_1 \rightarrow 0$,

$$\langle F \rangle = \frac{4(\Delta_0 - \delta_0)^2 \Omega^2 \Gamma_1 k_1 \cos\theta}{\bar{N}}, \quad (\text{A3})$$

where the denominator is $\bar{N} = 4(\Delta_0 - \delta_0)^2(4\Delta_0^2 + 2\Omega^2 + \Gamma_1^2) + 8(\delta_0 - \Delta_0)\Delta_0\bar{\Omega}^2 + (\Omega^2 + \bar{\Omega}^2)^2$ with the velocity-dependent detunings $\Delta_0 = \Delta - k_1v_z\cos\theta$ and $\delta_0 = \delta + k_2v_z\cos\theta\cos\bar{\theta}$. Here the velocity is defined as $v_z = z/t$. If we expand the force in Eq. (A3) around the point $v_z = 0$, i.e., $\langle F \rangle = F_0 - \beta v_z + O(v_z^2)$, a constant force is obtained by making $v_z = 0$ in $\langle F \rangle$, which reads $F_0 = 4(\Delta - \delta)^2 \Omega^2 \Gamma_1 k_1 \cos\theta / N$ with $N = 4(\Delta - \delta)^2(4\Delta^2 + 2\Omega^2 + \Gamma_1^2) + 8(\delta - \Delta)\Delta\bar{\Omega}^2 + (\Omega^2 + \bar{\Omega}^2)^2$. In this case, the friction coefficient turns out to be

$$\beta = 4\Omega^2 \Gamma_1 k_1 \cos^2\theta \left(\frac{N_2}{N} - \frac{N_1}{N^2} \right), \quad (\text{A4})$$

where $N_1 = 8(\Delta - \delta)^2[\bar{\Omega}^2(\delta k_1 - 2\Delta k_1 - \Delta k_2 \cos\bar{\theta}) + 4\Delta(\Delta - \delta)^2 k_1 + (\Delta - \delta)(k_1 + k_2 \cos\bar{\theta})(4\Delta^2 + 2\Omega^2 + \Gamma_1^2)]$ and $N_2 = 2(\Delta - \delta)(k_1 + k_2 \cos\bar{\theta})$.

In the absence of heating from the thermal bath, the final temperature after the Doppler cooling is determined

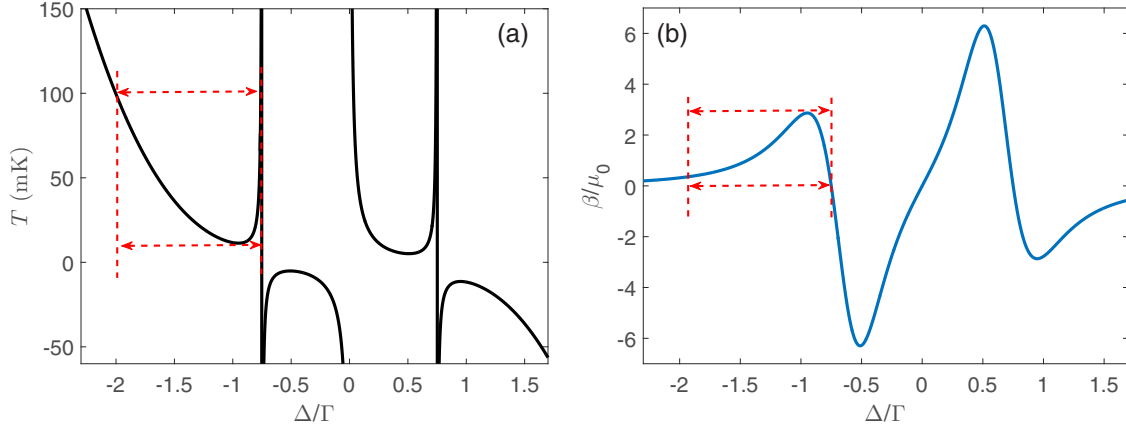


FIG. 4. (a) and (b) Final temperature T and friction coefficient β as a function of cooling laser detuning Δ , respectively, where the region framed by the red dashed lines represents the region under our experimental consideration. The negative value of temperature indicates a negative value of the friction coefficient, implying the heating effect instead of the cooling effect. Here the bath heating intensity is set as $E_e = 13\mu_0$ and other parameters are listed in the main text.

by $T_f = 2m^2D/2k_B\beta$ with the diffusion coefficient $D = k_1^2 \cos^2 \theta \Gamma_1 |\langle \sigma_y^{13} \rangle| / 4m^2$, which gives

$$T_f = \frac{\Gamma_1 (\Delta - \delta)^2}{2k_B \Omega N_h}, \quad (\text{A5})$$

where $N_h = N_2/k_1 \cos \theta - N_1/Nk_1 \cos \theta$. Under the heating from the surrounding environment, the ion's temperature is determined by

$$T = T_f + \frac{mE_e}{2k_B\beta}, \quad (\text{A6})$$

where E_e denotes the heating effect of the environment. In Fig. 4 we plot some numerical results of Eq. (A6) in a wide range of Δ . However, in our experiment, the cooling laser only works in the region as framed in Fig. 4. Moreover, it is difficult to make sure the point of zero detuning due to the large linewidth (23 MHz) of $|^4P_{1/2}\rangle$. Practically, we tried to determine the value of the critical detuning by sweeping Δ to the point that the temperature turns to be negative, i.e., appearance of heating effect. By this way, the zero detuning of the cooling laser is determined at $\Delta = -0.75\Gamma$.

Moreover, since both the incident lasers have the same intersection angles with the x axis, the friction coefficient can be calculated by Eq. (A5). However, in the y axis only the 866-nm laser with an intersection angle $\pi/2 - \bar{\theta}$ provides a friction coefficient which can be estimated as $\beta_y = \Gamma_2 k_2 \beta \sin \bar{\theta} / \Gamma_1 k_1 \cos \theta (\approx 0.0036\beta)$. Because the motions of the ions along the different direction are coupled, the final temperature in the three axes after Doppler cooling should be the same and can be estimated by calculating Eq. (A6).

APPENDIX B: DETERMINATION OF RABI FREQUENCY OF THE COOLING LASER

As presented above, the Rabi frequency Ω of the cooling laser is an important parameter for us to calculate the friction coefficient and the final temperature. However, due to the short lifetime of the excited state $|^4P_{1/2}\rangle$, the Rabi frequency Ω of the 397-nm laser is difficult to be measured in our

experiment. In contrast to the conventional way by observing the Rabi oscillation between the excited state $|^4P_{1/2}\rangle$ and the ground state $|^4S_{1/2}\rangle$, here we provide a method to measure the Rabi frequency of the cooling laser by experimentally observing the width of the detuning window between the point of zero detuning and the position at which the detuning creates the lowest temperature. The inset of Fig. 5 specifically presents how to carry out this estimation of Ω . The linear relation of the width of the detuning window with Ω , as demonstrated in Fig. 5, is obtained as $\Omega = (\Delta_w - w_2\Gamma)/w_1$ by the numerical simulation of the Langevin equation. We measure $\Delta_w = 40(6)$ MHz in our experiment, which means the Rabi frequency $\Omega = 78(17)$ MHz [i.e., $0.55(12)\Gamma$].

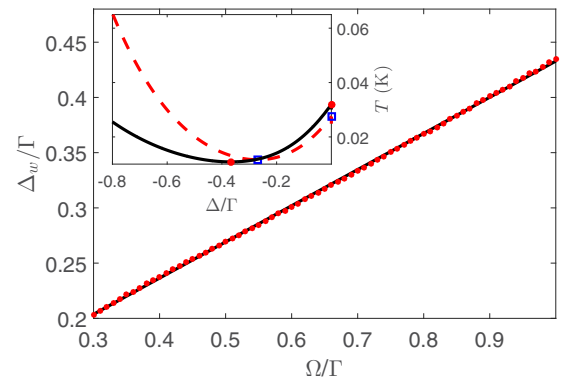


FIG. 5. Width Δ_w of the detuning window as a function of the Rabi frequency Ω of the cooling laser. The dots are the results of numerical simulation for different values of the Rabi frequency and the line is the corresponding linear fitting where the fitting function is $\Delta_w = w_1\Omega + w_2\Gamma$ with $w_1 = 0.344$ and $w_2 = 0.094$. (Inset) The ions' temperature as a function of the cooling laser detuning, where the dashed and the solid curves correspond to $\Omega/\Gamma = 0.5$ and 0.8 , respectively, and the two red dots (blue squares) label the positions of the minimum temperature and the zero detuning. Here the bath heating intensity is set as $E_e = 13\mu_0$.

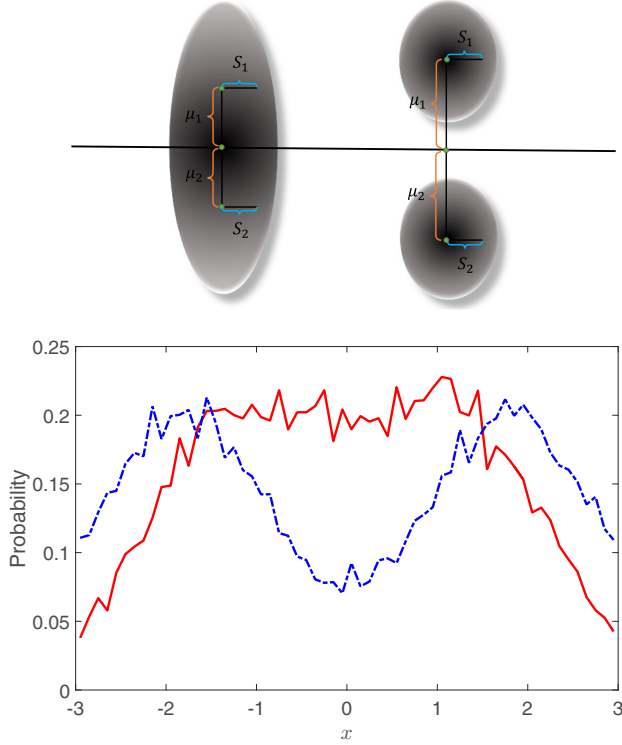


FIG. 6. (Top panel) Sketch for different images of the ions, where the left side is a blurring image due to an ion in a degenerate state before the structural phase transition occurs and the right side is the image for two separate states of an ion after the structural phase transition happens. We define a zero line, i.e., the horizontal line to separate the images as the two same halves. In both the images, each data above (below) the zero line has a dimensionless mean distance μ_1 (μ_2) and a mean square error S_1 (S_2). (Bottom panel) Exemplified curves for two different populations along the vertical direction of the horizontal line. For the red solid curve, $\mu_1 = 1.296$, $S_1 = 0.836$, $\mu_2 = -1.299$, $S_2 = 0.839$ and for the blue dashed curve, $\mu_1 = 1.837$, $S_1 = 0.968$, $\mu_2 = -1.851$, $S_2 = 0.949$.

APPENDIX C: IDENTIFYING MASS CENTERS OF THE IONS FROM THE EXPERIMENTAL IMAGES

Identifying the mass center of each ion from the data of the numerical simulation is an essential task. In this work, as sketched in Fig. 6, we develop a statistical method to determine the mass center of an ion. First, we define a statistical quantity U as

$$U = \frac{\mu_1 - \mu_2}{\sqrt{S_1^2 + S_2^2}} \rightarrow N(0, 1), \quad (\text{C1})$$

where $\mu_{1,2}$ and $S_{1,2}$ are defined in the caption of Fig. 6. Then, we select two options, $Q_0 : \mu_1 - \mu_2 = 0$, $Q_1 : \mu_1 - \mu_2 \neq 0$, controlled by the judgment value α . If $|U| \geq u_{1-\alpha/2}$, we reject Q_0 but choose Q_1 ; otherwise, we choose Q_0 . [Note u_{1-x} denotes the $1-x$ quantile of standard normal distribution which means $P(u > u_{1-x}) = x$, in other words, $\int_{u_{1-x}}^{\infty} p(u) du = x$ with $p(u)$ obeying the standard normal distribution, that is, $p(u) = e^{-u^2/2}/\sqrt{2\pi}$.] If $|U| \geq u_{1-\alpha/2}$, we consider that the ion is in the separate state of Fig. 6; otherwise, the ion is in the degenerate state. In our experiment, we take $\alpha = 0.02$,

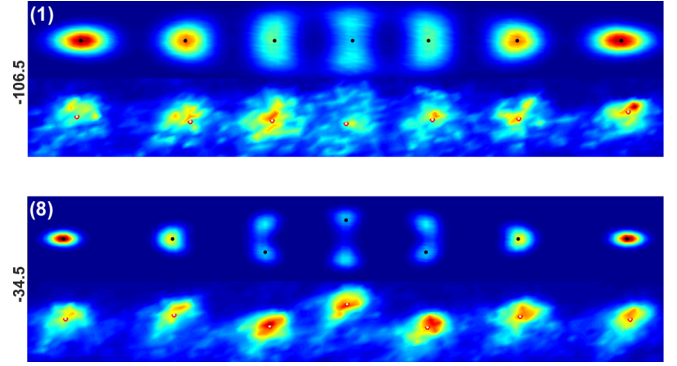


FIG. 7. Images of the ions selected from Fig. 2 of the main text, where the number in the vertical axis of each panel is the detuning Δ in units of MHz. The black dots are the ions' mass centers identified by our statistical method and the red hollow circles are obtained by the method for treating images involving background noise.

which gives $u_{0.99} = 2.32$. Taking the curves in Fig. 6 as an example, we have $U = 2.19$ for the red curve and $U = 2.75$ for the blue curve. Thus, we consider $\mu_1 - \mu_2 = 0$ for the red curve, implying that it is the left-side image in the top panel of Fig. 6. Meanwhile, we reject $\mu_1 - \mu_2 = 0$ for the blue curve and consider it showing another structure. Other examples can be found in Fig. 7, where panels (1) and (8) are identified as two different structures.

The above method works well for images in symmetry about a certain axis, where the datum of the ion's motional track is employed to identify the mass center of the ion. However, for the ion crystals located at different positions along the x axis, since the datum obtained experimentally is from spontaneous emission of the ions, which involves serious background noise, we have to first employ an extremum seeking method to find the seven peak values from

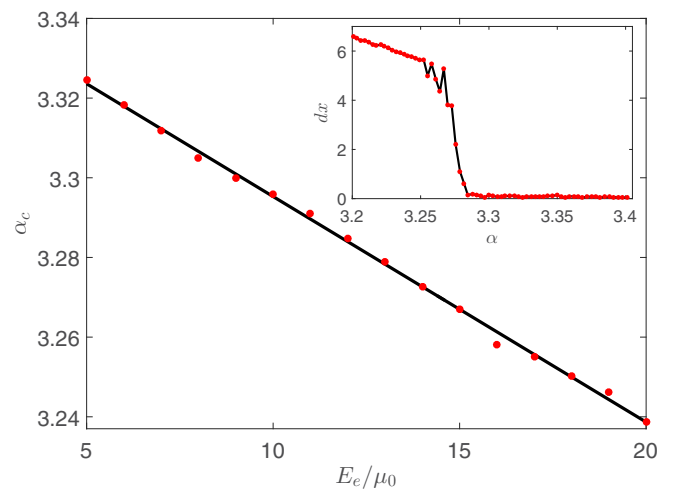


FIG. 8. Transition points α_c as a function of the bath heating strength E_e , where the detuning of the 397-nm laser is set as $\Delta = -30$ MHz. The dots are obtained by numerical calculation and the line is a linear fitting with $\alpha_c = aE_e + b$, in which $a = -0.0057$ and $b/\mu_0 = 3.352$. (Inset) A numerical calculation of the phase transition behavior as a function of the ratio α for $E_e/\mu_0 = 12$.

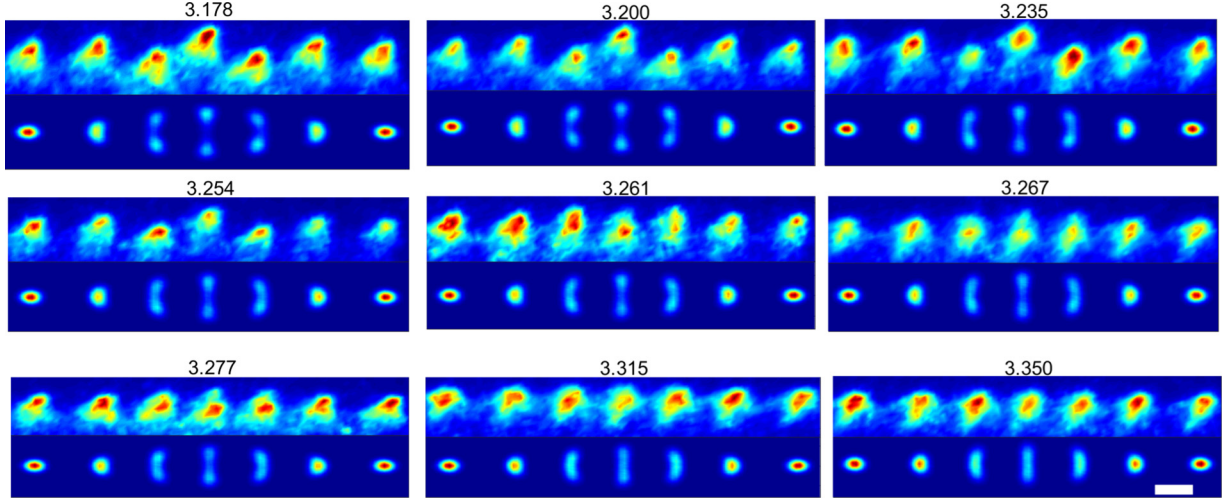


FIG. 9. Details of the structural phase transition by continuously sweeping α , where the number on the top of each panel is $\alpha = \omega_x/\omega_z$. The detuning of the 397-nm laser and bath heating intensity are set as $\Delta = -30$ MHz and $E_e/\mu_0 = 13$.

the fluorescence image, corresponding to the positions of the ions. Then we search the area of the $3\text{-}\mu\text{m}$ radius around each extremum point to find if the brightness is larger than 60% of the corresponding extremum point. Finally, within each of the areas, a weighted average over all the available data points is made to obtain the mean positions of the mass centers for different ions.

APPENDIX D: MOTION EQUATION OF IONS

For each of the trapped ions, the motion is given by the Langevin equation as below,

$$m\ddot{\vec{r}}_j + \beta\dot{\vec{r}}_j + \nabla_j\psi_j(\vec{r}_j) = \xi_j(t), \quad (\text{D1})$$

where m is the mass of the trapped j th ion with $\vec{r}_j = (x_j, y_j, z_j)$ being the coordinate, the total potential $\psi_j(\vec{r}_j)$ is the sum of all the dc potentials induced by the dc electrodes and the pseudopotential created by the rf electrodes [16], and β is the friction coefficient produced by the laser cooling. $\xi_j(t)$ is the stochastic force relevant to the temperature T obeying following ensemble average relations: $\langle \xi_j(t) \rangle =$

0 and $\langle \xi_j(t)\xi_k(\tau) \rangle = 2\eta k_B T \delta_{jk} \delta(t - \tau)$ with the Boltzmann constant k_B .

APPENDIX E: PRELIMINARY MEASUREMENTS

In our experiment, the bath heating is strong due to ions' temperature of 10–70 mK. To characterize the phase transition, measuring the bath heating strength E_e is a very important experimental premise. Besides, our experiment is started from the critical region of the structural phase transition. So determining the transition point in advance is necessary.

By numerical simulation for different bath heating, we find a linear relation of the transition points α_c with the bath heating intensity E_e , as plotted in Fig. 8. This means that, once we know the transition point α_c , we know uniquely the bath heating intensity E_e . Figure 3(d) of the main text presents a structural phase transition by sweeping α for a wide range, where the transition point $\alpha_c = 3.279(4)$ corresponds to $E_e = 13.0(8)\mu_0$. The images characterizing this phase transition process are demonstrated in Fig. 9.

- [1] S. An, J.-N. Zhang, M. Um, D. Lv, Y. Lu, J. Zhang, Z.-Q. Yin, H. T. Quan, and K. Kim, Experimental test of the quantum Jarzynski equality with a trapped-ion system, *Nat. Phys.* **11**, 193 (2015).
- [2] J. Roßnagel, S. T. Dawkins, K. N. Tolazzi, O. Abah, E. Lutz, F. Schmidt-Kaler, and K. Singer, A single-atom heat engine, *Science* **352**, 325 (2016).
- [3] A. Abdelrahman, O. Khosravani, M. Gessner, A. Buchleitner, H.-P. Breuer, D. Gorman, R. Masuda, T. Pruttivarasin, M. Ramm, P. Schindler, and H. Häffner, Local probe of single phonon dynamics in warm ion crystals, *Nat. Commun.* **8**, 15712 (2017).
- [4] T. P. Xiong, L. L. Yan, F. Zhou, K. Rehan, D. F. Liang, L. Chen, W. L. Yang, Z. H. Ma, M. Feng, and V. Vedral, Experimen-

tal Verification of a Jarzynski-Related Information-Theoretic Equality by a Single Trapped Ion, *Phys. Rev. Lett.* **120**, 010601 (2018).

- [5] J. M. R. Parrondo, J. M. Horowitz, and T. Sagawa, Thermodynamics of information, *Nat. Phys.* **11**, 131 (2015).
- [6] D. J. Wineland, J. C. Bergquist, W. M. Itano, J. J. Bollinger, and C. H. Manney, Atomic-Ion Coulomb Clusters in an Ion Trap, *Phys. Rev. Lett.* **59**, 2935 (1987).
- [7] W. M. Itano, J. J. Bollinger, J. N. Tan, B. Jelenković, X.-P. Huang, and D. J. Wineland, Bragg diffraction from crystallized ion plasmas, *Science* **279**, 686 (1998).
- [8] M. Drewsen, C. Brodersen, L. Hornekaer, J. S. Hangst, and J. P. Schiffer, Large Ion Crystals in a Linear Paul Trap, *Phys. Rev. Lett.* **81**, 2878 (1998).

- [9] D. H. E. Dubin and T. M. O. Neil, Trapped nonneutral plasmas, liquids, and crystals (the thermal equilibrium states), *Rev. Mod. Phys.* **71**, 87 (1999).
- [10] J. P. Schiffer, Phase Transitions in Anisotropically Confined Ionic Crystals, *Phys. Rev. Lett.* **70**, 818 (1993).
- [11] D. H. E. Dubin, Theory of Structural Phase Transitions in a Trapped Coulomb Crystal, *Phys. Rev. Lett.* **71**, 2753 (1993).
- [12] D. G. Enzer, M. M. Schauer, J. J. Gomez, M. S. Gulley, M. H. Holzscheiter, P. G. Kwiat, S. K. Lamoreaux, C. G. Peterson, V. D. Sandberg, D. Tupa, A. G. White, R. J. Hughes, and D. F. V. James, Observation of Power-Law Scaling for Phase Transitions in Linear Trapped Ion Crystals, *Phys. Rev. Lett.* **85**, 2466 (2000).
- [13] L. Hornekær, N. Kjærgaard, A. M. Thommesen, and M. Drewsen, Structural Properties of Two-Component Coulomb Crystals in Linear Paul Traps, *Phys. Rev. Lett.* **86**, 1994 (2001).
- [14] N. Kjærgaard and M. Drewsen, Observation of a Structural Transition for Coulomb Crystals in a Linear Paul Trap, *Phys. Rev. Lett.* **91**, 095002 (2003).
- [15] A. Mortensen, E. Nielsen, T. Matthey, and M. Drewsen, Observation of Three-Dimensional Long-Range Order in Small Ion Coulomb Crystals in an Rf Trap, *Phys. Rev. Lett.* **96**, 103001 (2006).
- [16] L. L. Yan, W. Wan, L. Chen, F. Zhou, S. J. Gong, X. Tong, and M. Feng, Exploring structural phase transitions of ion crystals, *Sci. Rep.* **6**, 21547 (2016).
- [17] Z.-X. Gong, G.-D. Lin, and L.-M. Duan, Temperature-Driven Structural Phase Transition for Trapped Ions and a Proposal for its Experimental Detection, *Phys. Rev. Lett.* **105**, 265703 (2010).
- [18] J. Z. He, L. L. Yan, L. Chen, J. Li, and M. Feng, Measurement of heating rates in a microscopic surface-electrode ion trap, *Chin. Phys. Lett.* **34**, 063701 (2017).
- [19] M. Brownnutt, M. Kumph, P. Rabl, and R. Blatt, Ion-trap measurements of electric-field noise near surfaces, *Rev. Mod. Phys.* **87**, 1419 (2015).
- [20] M. Marcianti, C. Champenois, A. Calisti, J. Pedregosa-Gutierrez, and M. Knoop, Ion dynamics in a linear radio-frequency trap with a single cooling laser, *Phys. Rev. A* **82**, 033406 (2010).
- [21] Besides the laser cooling effect shared from other directions due to the angle of $\pi/36$, the cooling in the y axis is also benefited from the coupling of the motional degrees of freedom between different directions. This can be understood from our previous study in H.-Y. Wu, Y. Xie, W. Wan, L. Chen, F. Zhou, and M. Feng, A complicated Duffing oscillator in the surface-electrode ion trap, *Applied Physics B* **114**, 81 (2014).
- [22] Y. Ibaraki, U. Tanaka, and S. Urabe, Detection of parametric resonance of trapped ions for micromotion compensation, *Appl. Phys. B* **105**, 219 (2011).
- [23] S. Fishman, G. De Chiara, T. Calarco, and G. Morigi, Structural phase transitions in low-dimensional ion crystals, *Phys. Rev. B* **77**, 064111 (2008).
- [24] G. Alzetta, A. Gozzini, L. Moi, and G. Orriols, Experimental method for observation of RF transitions and laser beat resonances in oriented Na vapor, *Il Nuovo Cimento B Series* **36**, 5 (1976).
- [25] E. Arimondo and G. Orriols, Non-absorbing atomic coherences by coherent 2-photon transitions in a 3-level optical pumping, *Let. Nuovo Cimento* **17**, 333 (1976).
- [26] E. Arimondo, Coherent population trapping in laser spectroscopy, *Prog. Opt.* **35**, 257 (1996).
- [27] C. Lisowski, M. Knoop, C. Champenois, G. Hagel, M. Vedel, and F. Vedel, Dark resonances as a probe for the motional state of a single ion, *Appl. Phys. B* **81**, 5 (2005).
- [28] D. Reiß, K. Abich, W. Neuhauser, C. Wunderlich, and P. E. Toschek, Raman cooling and heating of two trapped Ba^+ ions, *Phys. Rev. A* **65**, 053401 (2002).
- [29] J. Roßnagel, K. N. Tolazzi, F. Schmidt-Kaler, and K. Singer, Fast thermometry for trapped ions using dark resonances, *New J. Phys.* **17**, 045004 (2015).
- [30] F. Diedrich, E. Peik, J. M. Chen, W. Quint, and H. Walther, Observation of a Phase Transition of Stored Laser-Cooled Ions, *Phys. Rev. Lett.* **59**, 2931 (1987).
- [31] R. Blümel, J. M. Chen, E. Peik, W. Quint, W. Schleich, Y. R. Shen, and H. Walther, Phase transitions of stored laser-cooled ions, *Nature (London)* **334**, 309 (1988).
- [32] R. Blümel, C. Kappler, W. Quint, and H. Walther, Chaos and order of laser-cooled ions in a Paul trap, *Phys. Rev. A* **40**, 808 (1989).
- [33] D. J. Evans, E. G. D. Cohen, and G. P. Morriss, Probability of Second Law Violations in Shearing Steady States, *Phys. Rev. Lett.* **71**, 2401 (1993).
- [34] D. J. Evans and D. J. Searles, The fluctuation theorem, *Adv. Phys.* **51**, 1529 (2002).
- [35] E. Shimshoni, G. Morigi, and S. Fishman, Quantum Zigzag Transition in Ion Chains, *Phys. Rev. Lett.* **106**, 010401 (2011).
- [36] R. Schmied, T. Roscilde, V. Murg, D. Porras, and J. I. Cirac, Quantum phases of trapped ions in an optical lattice, *New J. Phys.* **10**, 045017 (2008).
- [37] A. Bermudez, J. Almeida, F. Schmidt-Kaler, A. Retzker, and M. B. Plenio, Frustrated Quantum Spin Models with Cold Coulomb Crystals, *Phys. Rev. Lett.* **107**, 207209 (2011).
- [38] K. Modi, A. Brodutch, H. Cable, T. Paterek, and V. Vedral, The classical-quantum boundary for correlations: Discord and related measures, *Rev. Mod. Phys.* **84**, 1655 (2012).
- [39] D. Podolsky, E. Shimshoni, P. Silvi, S. Montangero, T. Calarco, G. Morigi, and S. Fishman, From classical to quantum criticality, *Phys. Rev. B* **89**, 214408 (2014).